JMEPEG (2012) 21:1440–1446
DOI: 10.1007/s11665-011-0016-z

1059-9495/$19.00

The Study of Nano-Sized Carbide Particles Formed in Fe-Cr-W-V Alloy

Abdul Javad Novinrooz, Samira Moniri, Mohsen Asadi Asadabad, and Alireza Hojabri

(Submitted September 5, 2010; in revised form June 26, 2011)

The microstructural features of nanocarbide particles formed in Fe-Cr-W-V alloy were studied. A Fe-Cr-W-V alloy was first heat treated under different conditions. In this study, optical microscopy, scanning and transmission electron microscopy, x-ray diffraction, and hardness tester were used. The shape, size distribution, type, and lattice parameters of the extracted particles were investigated. The identified carbides were MC, M_7C_3, and $M_{23}C_6$. The particle size measurements showed that the mean length of carbide particles during 0.5, 5, and 20 h was about 103, 128, and 142 nm, respectively. Also, the mean thickness of carbide particles during 0.5, 5, and 20 h was about 54, 67, and 74 nm, respectively.

Keywords carbide particles, lattice parameter, size distribution, x-ray diffraction

1. Introduction

Fast-induced radioactivity decay Fe-Cr-W-V alloys are new high-strength materials suitable for the use in fusion reactor applications (Ref 1). Because of the effect of service environment (such as stress, rupture, creep, and irradiation) on material operation at elevated temperatures, microstructure of these alloys must be resistant to damage that may form defect structures. Thus, the composition and heat treatment of Fe-Cr-W-V alloys should be modified (Ref 2). A heat treatment includes normalizing and tempering processes at 600 and 700 °C to cause the microstructural stability of Fe-Cr-W-V alloys and optimization of their mechanical properties (Ref 3). Also, normalizing and tempering provide a large number of nucleation sites for carbide particles. After tempering, dispersion of carbide particles takes place in the matrix of the alloy (Ref 4). Carbide phases are made up of many elements. To describe the chemical formula, a plain notation system is applied with "M" showing the metal content and "X" as carbon or nitrogen (Ref 3, 5). In Fe-Cr-W-V alloys, Cr, W, and V elements are strong carbide formers and improve the alloy's mechanical properties such as hardness and creep strength at high temperatures. V is the main element that forms MC-type carbide particles and increases hardenability (Ref 6). Presence of W delays the coarsening of $M_{23}C_6$ carbide particles (Ref 7). C is necessary to make carbide particles and Cr improves the corrosion resistance (Ref 8). These elements are needed to create fine carbide particles such as M_3C, $M_{23}C_6$, M_7C_3, M_6C, M_2C, and MC after tempering treatment. These carbide particles show the diversities of morphology and crystal structure conformably to the chemical composition and heat-treatment conditions, and provide high-strength levels at elevated temperatures (Ref 9). Therefore, precipitation of nanocarbide particles stabilizes the microstructure of Fe-Cr-W-V alloys. Controlling of the nanocarbide particles distribution is an essential factor for the recovery of revenue Fe-Cr-W-V alloys (Ref 10). The purpose of this study is the identification of carbide particles by TEM and XRD techniques.

Abdul Javad Novinrooz and **Mohsen Asadi Asadabad**, Materials Research School, NSTRI, Karaj, Iran; and **Samira Moniri** and **Alireza Hojabri**, Department of Physics, Karaj Branch, Islamic Azad University, Karaj, Iran. Contact e-mail: sss_moniri@yahoo.com.

2. Experimental Procedure

The chemical composition of Fe-Cr-W-V alloy was Fe-0.091% C-4.37% Cr-1.91% W-0.28% V (wt.%). The austenitizing and tempering treatments were performed at 1000 °C (for 0.5 h) and 700 °C (for 0.5, 5, and 20 h), respectively. The specimens of size $10 \times 10 \times 10$ mm^3 were prepared. The specimens were hot-mounted, polished, and etched using 4% (vol.%) nitric acid in ethanol. The microstructural observations were carried out using optical microscope (Leitz model), scanning electron microscope (Philips XL-30), and transmission electron microscope (Philips-EM-208S). Rockwell hardness was measured by using the loads up to 60 kg. The precipitated particles were electrolytically separated from the matrix of Fe-Cr-W-V alloy. The X-ray diffraction (XRD) analysis was performed by a Philips-PW 1800 diffractometer. The lattice parameter of specimens was determined by XRD analysis and using X'Pert High Score software. The details of the experimental procedure have been given in our previous work (Ref 3).

3. Results and Discussion

3.1 Optical Microscopy

The optical micrographs of the specimens tempered at 700 °C for 0.5, 5, and 20 h are shown in Fig. 1(a)-1(c). The optical observations confirmed that all microstructures at this

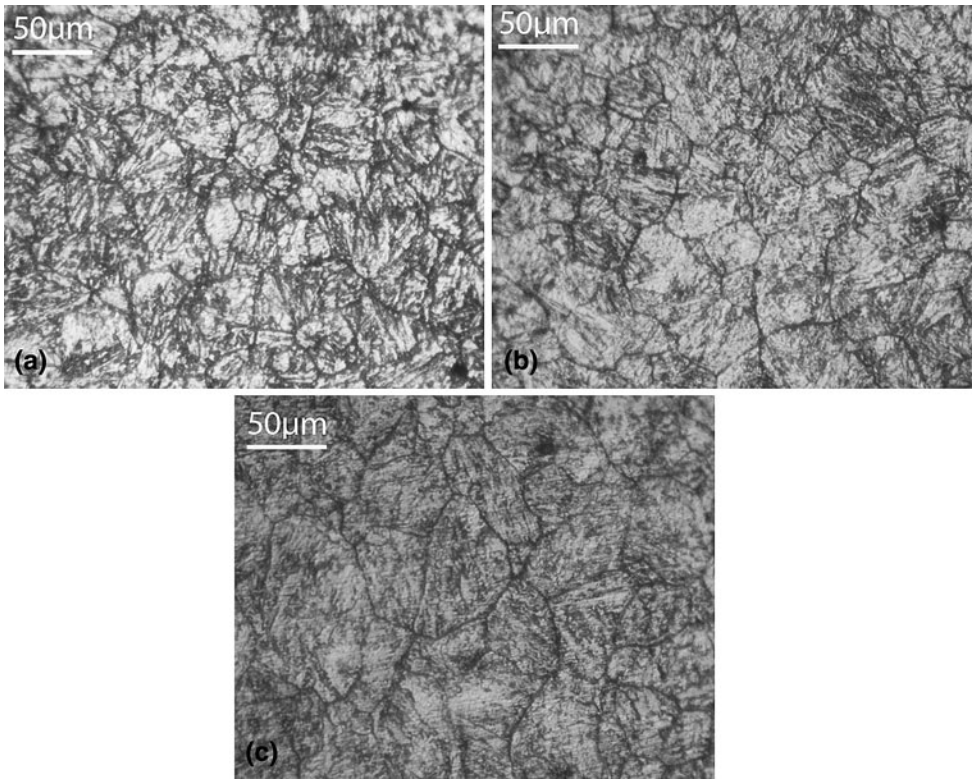

Fig. 1 Optical micrographs of the specimens of Fe-Cr-W-V alloy tempered at 700 °C for (a) 0.5, (b) 5, and (c) 20 h

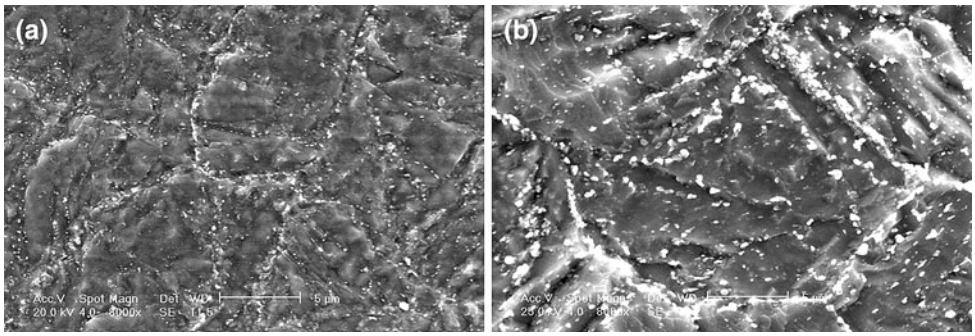

Fig. 2 SEM micrographs of the specimens of Fe-Cr-W-V alloy tempered at 700 °C for (a) 0.5 and (b) 20 h

magnification range showed a tempered martensitic lath structure at all heat-treatment conditions. Also, the formation sites of the nanocarbide particles were boundaries of martensite laths and lath packets (Ref 11). As tempering time increased, the prior austenite-grain size was increased as well (Fig. 1a-c). Optical microscopy is not able to clearly assess the precipitation condition of the carbide particles (Ref 12).

3.2 Scanning Electron Microscopy

The SEM microstructural images of the specimens tempered at 700 °C for 0.5 and 20 h are shown in Fig. 2(a) and 2(b), respectively. Precipitation of nanocarbide particles within the tempered martensitic laths and also along the grain boundaries is clearly noticeable in Fig. 2(a) and 2(b). This is acceptable, because precipitation potential of the nanoparticles in the boundaries is higher than in the other places. In addition, as shown in Fig. 2(b), the increasing of tempering time resulted in the growth of nanocarbide particles. In other words, the sizes of nanocarbide particles in the grain and lath boundaries as result of tempering for 0.5 h are smaller than those tempered for 20 h. Moreover, the number density of precipitates in the sample tempered for 20 h is higher than the one tempered for 0.5 h.

3.3 Transmission Electron Microscopy

The TEM micrographs of the specimens tempered at 700 °C for 5 and 20 h are presented in Fig. 3(a) and 3(b). As shown, the carbide particles morphology varies from blocky, spherical, and needle to irregular geometrical shapes. Also, they have considerably different sizes. Differences of carbide particles in shape and size can be a guide for their identification as well (Ref 13). Few spherical carbide particles were detected in the TEM micrographs (with a diameter of about 40 nm) (Fig. 3b). Figure 3(c) and 3(d) represents the electron diffraction pattern of blocky and spherical nanocarbide particles, respectively.

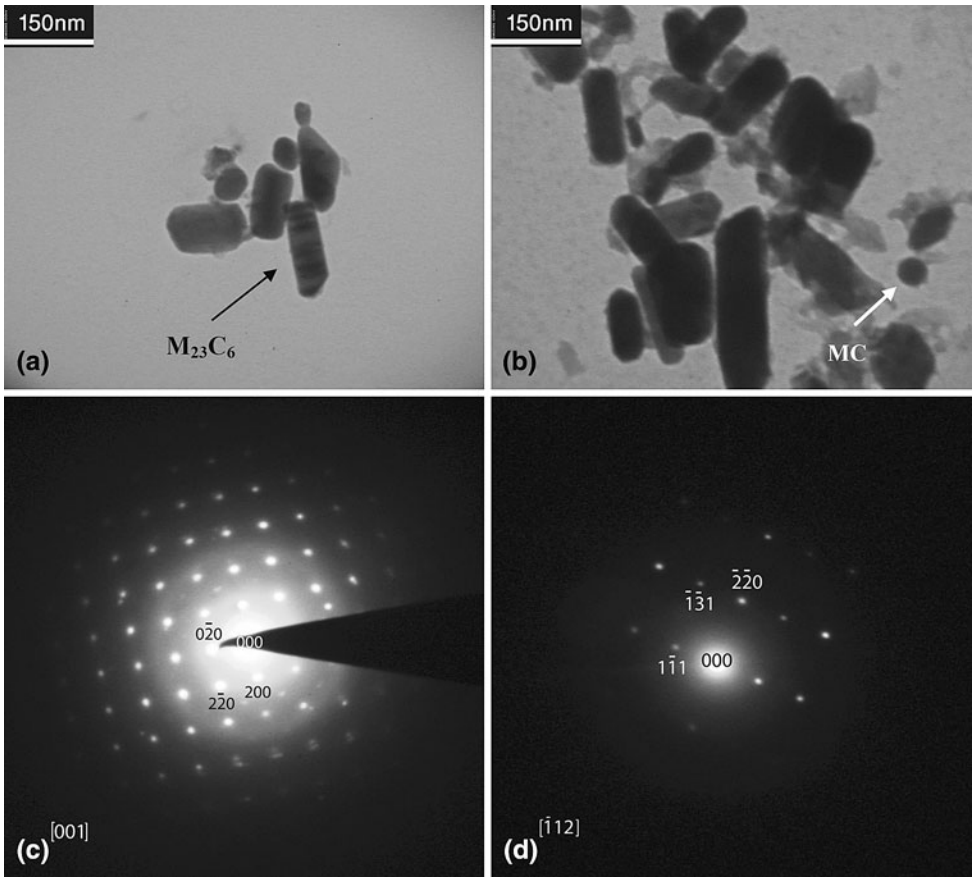

Fig. 3 (a, b) The TEM micrographs of carbide particles of the specimens tempered at 700 °C for 5 and 20 h. (c, d) The electron diffraction patterns corresponding to the particles shown by arrow in (a) and (b), respectively

Since, the lattice parameters of $M_{23}C_6$ ($a \approx 10.58$ Å) and MC ($a \approx 4.71$ Å) are different, therefore, by analyzing the electron diffraction pattern, the $M_{23}C_6$ and MC carbides were identified. Similar to the previous reports, V-rich MC carbide particles were also seen in 7Cr-2WVTa and 9Cr-2WVTa alloys after tempering at 750 °C (Ref 14).

Tempering at 700 °C mainly ends with blocky-shaped particles in the alloy. Therefore, the size distribution curves were plotted as the length and thickness of the carbide particles. Since, each alloy carbide particle grows at a different rate, the size of carbide particles is different as well (Ref 15). Further, particle size depends on the nucleation parameters such as nucleation sites. On the other hand, particle size distributions are useful to discuss the influence of particle size on the creep of alloys (Ref 16). Therefore, using TEM micrographs, the size of carbide particles for the tempered alloy was determined directly at different conditions. The carbide particle sizes were measured by at least 550 particles in each heat treatment. The obtained data were then plotted as a function of time to estimate the average size of the carbide particles. Size distributions of the carbide particles against tempering time are plotted in Fig. 4 and 5. Figure 4 shows the length distribution of carbide particles for the specimens tempered at 700 °C for 0.5, 5, and 20 h. As seen, the length of carbide particles in the specimens tempered for 0.5, 5, and 20 h is in the size range of 30-270 nm, 30-330 nm, and 30-400 nm, respectively. Also, the mean length of the carbide particles tempered for 0.5, 5, and 20 h is about 103, 128, and 142 nm, respectively. The thickness distributions of the carbide particles in the specimens tempered for 0.5, 5, and 20 h are presented in Fig. 5. The thicknesses of carbide particles during the 0.5, 5, and 20 h tempering is in the size range of 20-120 nm, 30-160 nm, and 20-180 nm, respectively. Also the mean thicknesses of carbide particles for 0.5, 5, and 20 h tempering is about 54, 67, and 74 nm, respectively. The specimen tempered for 0.5 h has the smallest particle size, thus it has the most severe increase in particle hardening. Comparison of the size distributions of the specimens at different times clearly shows that the size of carbide particles has a direct relation with tempering time. So that by increasing of tempering time, the carbide particles become coarse. The coarsening of carbide particles in Fe-Cr-W-V alloys is an important factor that considerably influences their mechanical properties.

3.4 X-ray Diffraction

The important factors such as lattice parameter, crystal structure, volume fraction changes, and type of the extracted carbide particles were characterized by XRD analysis. Figure 6 shows the XRD patterns of the specimens tempered at 700 °C for 0.5, 5, and 20 h. The difference in the peak intensities of the sample tempered for 5 h with other samples may be due to more amount of material, which was taken during the XRD test. It is clear from Fig. 6, that, in all the specimens, the strongest peak belongs to $M_{23}C_6$. This shows the higher stability of this carbide particle in Fe-Cr-W-V alloy. Based on the mentioned

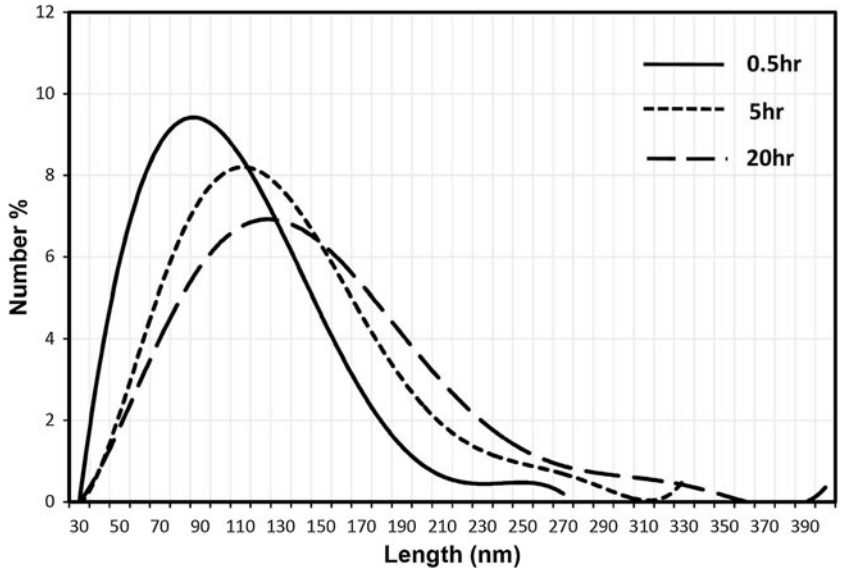

Fig. 4 Length distribution of the carbide particles of specimens tempered at 700 °C for 0.5, 5, and 20 h

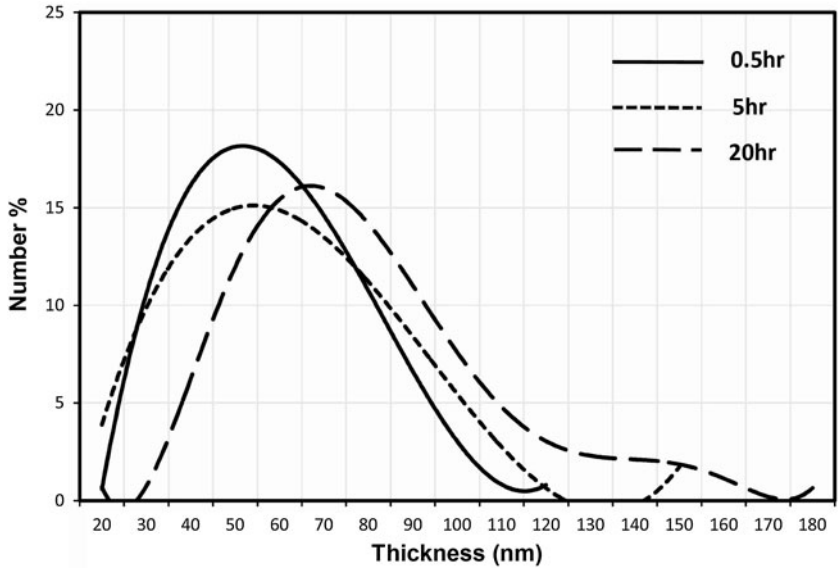

Fig. 5 Thickness distribution of the carbide particles of specimens tempered at 700 °C for 0.5, 5, and 20 h

patterns, one can clearly identify $M_{23}C_6$ and M_7C_3 peaks, but since the diffraction peaks of MC are not sharp, they can hardly be seen in all samples. The amount of MC carbide particles in comparison to those of M_7C_3 and $M_{23}C_6$ is too low. Therefore, the peak intensity of MC particles is weaker. Amount of MC carbide particles observed in the TEM micrographs was also very low. Further, Danon and Servant (Ref 14) identified the $M_{23}C_6$, M_7C_3, and V(C, N) carbide particles in 5Cr-2WVTa alloy after tempering at 750 °C. In Cr-containing alloys, by the advance of tempering, M_7C_3 dissolves and transforms into $M_{23}C_6$ (Ref 14). Therefore, in these alloys, $M_{23}C_6$ is a stable and M_7C_3 is a metastable carbide particle. The crystal structures of $M_{23}C_6$, M_7C_3, and MC identified by XRD analysis are fcc, trigonal, and fcc, respectively.

The relative amounts of $M_{23}C_6$ and M_7C_3 were calculated by XRD intensity ratio to that of MC = $([MC_{(111)} + MC_{(200)}]/2)$ as follows (the intensity of MC was the same at all conditions):

$$M_{23}C_6 = [\{M_{23}C_{6\,(420)} + M_{23}C_{6\,(422)} + M_{23}C_{6\,(440)}\}/3]/MC$$

$$M_7C_3 = [\{\ M_7C_{3\,(420)} + M_7C_{3\,(501)} + M_7C_{3\,(440)}\}/3]/MC$$

This method was also used in other studies (Ref 9).

In fact, the peak intensity of the carbide phases depends on their amount in the alloy (Ref 12). The relative amounts of $M_{23}C_6$ and M_7C_3, according to the XRD data, as a function of tempering time are shown in Fig. 7.

It can be clearly seen in Fig. 7 that as tempering time increases from 0.5 to 20 h, the relative amount of $M_{23}C_6$ increases and at the same time, the amount of M_7C_3 decreases. This confirms that $M_{23}C_6$ is the most stable carbide particle in this alloy at 700 °C and that M_7C_3 is metastable thermodynamically. Also, using the

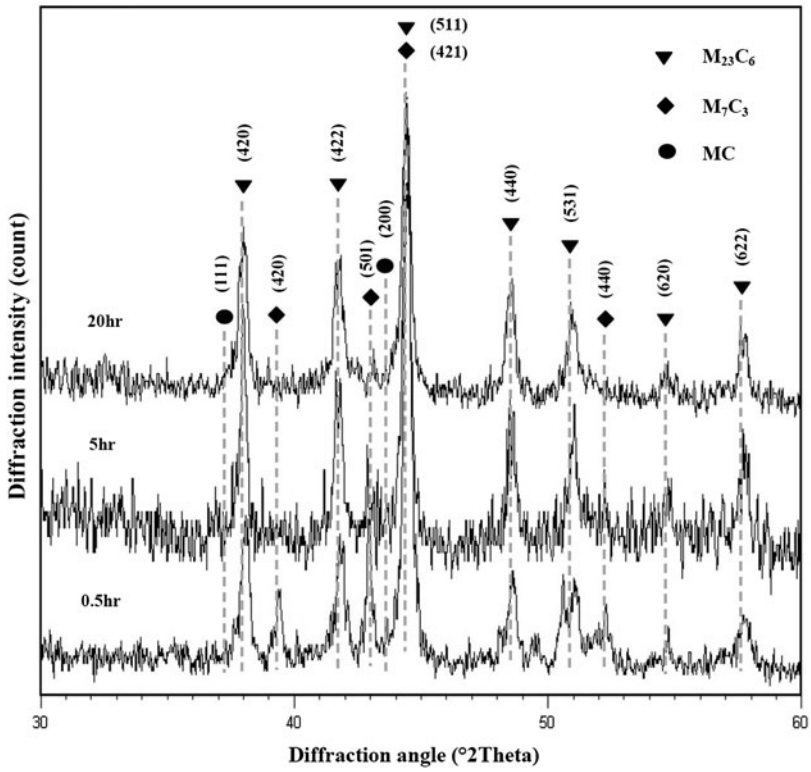

Fig. 6 XRD patterns of the extracted carbide particles of the specimens tempered at 700 °C for 0.5, 5, and 20 h, respectively

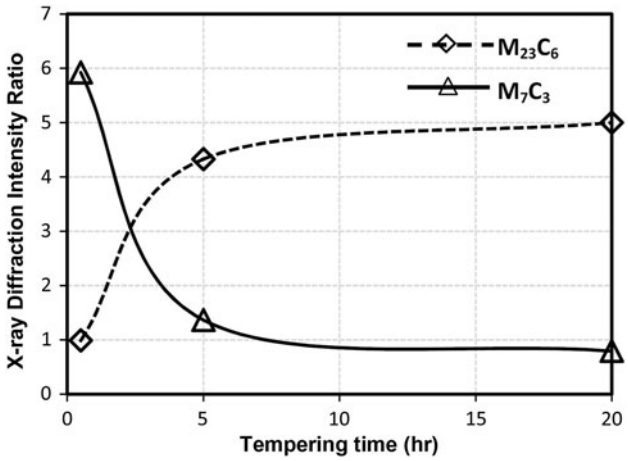

Fig. 7 Relative amount changes of $M_{23}C_6$ and M_7C_3 of the specimens tempered at 700 °C for 0.5, 5, and 20 h

thermodynamic parameters such as ΔG, the stability and transformation behavior of carbides can be easily understood. According to the Ref 17, $\Delta G_{M_{23}C_6} < \Delta G_{M_7C_3}$ in 2.25 Cr-1.6 W-V-Nb alloy. On the other hand, $M_{23}C_6$ is more stable than M_7C_3 thermodynamically. Therefore, M_7C_3 dissolves when tempering time increases and transforms into stable $M_{23}C_6$ carbide. In addition, the dissolution rate of M_7C_3 is high at this temperature, which is in agreement with our experimental findings.

The lattice parameters of MC and $M_{23}C_6$ as well as the lattice parameter ratio (a/c) of M_7C_3 as a function of tempering time are shown in Fig. 8. By increasing of tempering time, the lattice parameters of $M_{23}C_6$ and MC were increased and the lattice parameter ratio of M_7C_3 was decreased. It is well known that different parameters such as diffusion of carbon and alloy elements would change the lattice parameters (Ref 18). As MC is vanadium rich carbide, by increasing of tempering time, more vanadium will penetrate into the lattice, resulting in lattice distortion. Hence, MC lattice parameter will increase (Fig. 8c). Similarly, by increasing of tempering time, the Cr/Fe ratio of $M_{23}C_6$ will increase. As a result, Cr amount in the lattice of $M_{23}C_6$ will increase and thus, the lattice parameter will increase as well (Fig. 8a). However, in M_7C_3 carbide, as mentioned already, the alloy elements diminish; therefore, the lattice parameter ratio of M_7C_3 decreases (Fig. 8b).

3.5 Hardness Measurements

Figure 9 shows the tempering curve of the Fe-Cr-W-V alloy hardness at 700 °C. As shown, the hardness is dropped linearly by increasing of tempering time. The main reason is that with the advance of tempering, a slight softening occurs in the matrix microstructure. Another reason could be that the nanocarbide particles continue to coarsen with the increasing of tempering time, as discussed in the Section 3.3.

4. Conclusions

The microstructural features of nanocarbide particles formed in Fe-Cr-W-V alloy austenitized at 1000 °C and tempered at 700 °C for 0.5, 5, and 20 h were studied. By extraction of carbide particles, their size, shape, type, lattice parameter, crystal structure, and relative amount changes were determined by TEM, electron diffraction, and XRD analyses. Also, microstructural considerations were done using OM and SEM

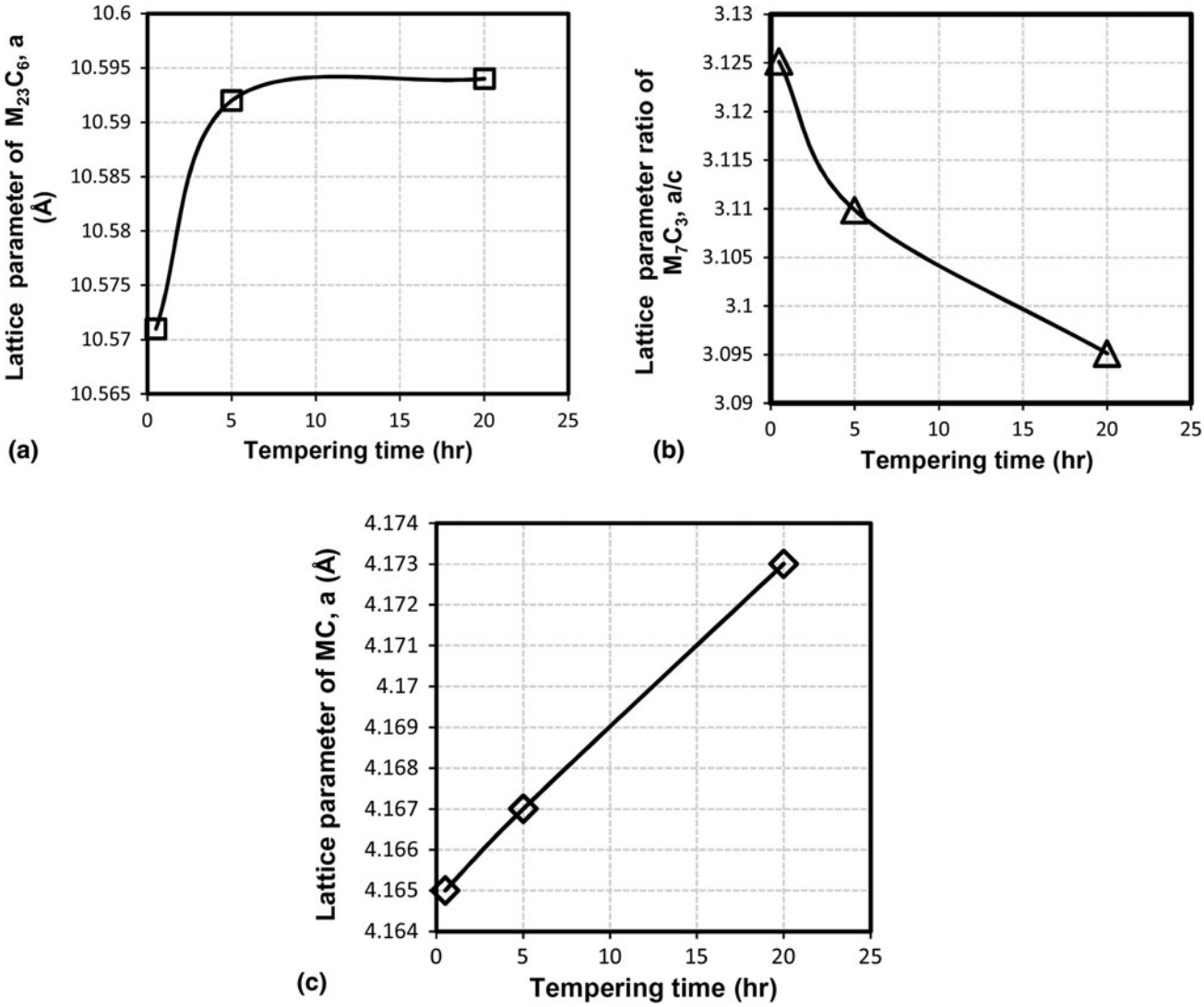

Fig. 8 The lattice parameter changes of (a) $M_{23}C_6$, (b) M_7C_3, and (c) MC carbide particles

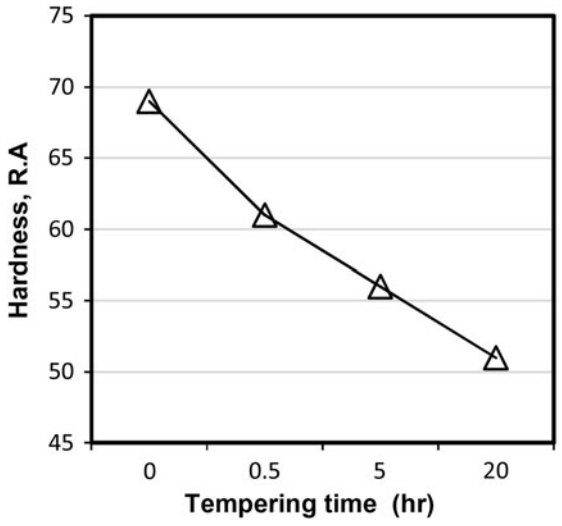

Fig. 9 The rockwell hardness number as a function of tempering time

analyses. Furthermore, hardness measurements were performed on all specimens. The results showed that the microstructure of alloy after tempering at different heat-treatment conditions was tempered martensite. By XRD analysis, $M_{23}C_6$, M_7C_3, and MC particles were identified, and confirmed by electron diffraction patterns. The mean length of the carbide particles after 0.5, 5, and 20 h of tempering was determined as about 103, 128, and 142 nm, respectively. Also, the mean thickness of the carbide particles after 0.5, 5, and 20 h of tempering was about 54, 67, and 74 nm, respectively. The hardness observations showed that when tempering time increases, the hardness of Fe-Cr-W-V alloy decreases.

References

1. P. Fernandez, M. Garc-Mazar, A.M. Lancha, and J. Lapena, Grain Boundary Microchemistry and Metallurgical Characterization of Eurofer'97 after Simulated Service Conditions, *J. Nucl. Mater.*, 2004, **329-333**, p 273–277

2. J. Janovec, M. Svoboda, and J. Blach, Evolution of Secondary Phases During Quenching and Tempering 12% Cr Steel, *Mater. Sci. Eng. A.*, 1998, **249**, p 184–189
3. M. Asadi Asadabad, S. Kheirandish, and A. Novinrooz, Microstructural and Mechanical Behavior of 4.5 Cr-2 W-0.25 V-0.1 C Steel, *Mater. Sci. Eng. A*, 2010, **527**, p 1612–1616
4. D.V. Shtansky, K. Nakai, and Y. Ohmori, Decomposition of Martensite by Discontinuous Like Precipitation Reaction in a Fe-17 Cr-0.5 C Alloy, *Acta Mater.*, 2000, **48**, p 969–983
5. D.G. Cole, "Design of Heat Resistant Steels for Small Power Plant," Thesis, Department of Mater. Sci. Metall., University of Cambridge, 2000
6. V. Gaffard, "Experimental Study and Modelling of High Temperature Creep Flow and Damage Behavior of 9Cr1Mo-NbV Steel Weldments," Thesis, Ingénieur de l'Institut National Polytechnique de Grenoble, 2007
7. S.G. Hong, W.B. Lee, and C.G. Park, The Effects of Tungsten Addition on the Microstructural Stability of 9Cr-Mo Steels, *J. Nucl. Mater.*, 2001, **288**, p 202–207
8. E. Manilova, *Examination of Minor Phases in Martensitic 12% Cr-Mo-W-V Steel*, Microscopy Society of America, Polzunov Central Boiler and Turbine Institute, 2006, p 1612–1613
9. K. Miyata, M. Igarash, and Y. Sawaragi, Effect of Trace Elements on Creep Properties of 0.06 C-2.25 Cr-1.6 W-0.1 Mo-0.25 V-0.05 Nb Steel, *ISIJ. Int.*, 1999, **39**(9), p 947–954
10. M. Tamura, H. Kusuyama, K. Shinozuka, and H. Saka, Tempering Process and Precipitation Behavior of 8% Cr-2% WTa Steel, *ISIJ Int.*, 2007, **47**(2), p 317–326
11. M.V. Leonteva-Smirnova, A.G. Ioltukhovskiy, G.A. Arutiunova, A.V. Tselischev, and V.M. Chernov, Investigation of Heat Treatment Conditions on the Structure of 12% Chromium Reduced Activation Steels, *J. Nucl. Mater.*, 2002, **307-311**, p 466–470
12. A. Baltusnikas and R. Levinskas, XRD Analysis of Carbide Phase in Heat Resistant Steels, *Mater. Sci.*, 2006, **12**(3), p 192–198
13. R.D. Fu, T.S. Wang, W.H. Zhou, W.H. Zhang, and F.C. Zhang, Characterization of Precipitates in 2.25 Cr-1 Mo-0.25 V Steel for Large-Scale Cast-Forged Products, *Mater. Charact.*, 2007, **58**, p 968–973
14. C.A. Danon and C. Servant, Thermodynamic Modeling in Reduced Activation Steels, *ISIJ Int.*, 2005, **45**(6), p 903–912
15. N. Fujita, "Modeling of Carbide Precipitation in Alloy Steels," Thesis, Department of Mater. Sci. Metall., University of Cambridge, 2000
16. H. Magnusson, "Creep Modeling of Particle Strengthened Steels," Thesis, Department of Mater. Sci. Metall., Royal Institute of Technology, 2007
17. L. Zhu and M.A. Xueming, Microstructural Evolution of 2.25 Cr-1.6 W-V-Nb Heat Resistant Steel During Creep, *J. Mater. Sci. Technol.*, 2003, **19**(2), p 126–128
18. A. Baltusnikas, R. Levinskas, and I. Lukosiute, Analysis of Heat Resistant Steel State by Changes of Lattices Parameters of Carbides Phases, *J. Mater. Sci.*, 2008, **14**(3), p 210–214